Restoration of tumor suppressor protein with enhanced activity using super-tRNAs to induce tumor regression

Bangyan Kong[1,2#], Zhetao Zheng[1,2#], Zeyuan Mi[1,2], Zhiyang Dou[1,2], Yuelin Yang[1], Yuxuan Shen[1], Liangzhen Dong[1,2], Jingru Lv[1,2], Ying Li[1,2], Qing Liang[1,2], Songlin Tian[2], Jiayu Wang[1,2], Hua Qiao[1,2], Qing Xia[1,2]✉

1. State Key Laboratory of Natural and Biomimetic Drugs, Peking University, Beijing, 100191, China.

2. Department of Molecular and Cellular Pharmacology, School of Pharmaceutical Sciences, Peking University, Beijing, 100191, China.

# These authors contributed equally to this work.

✉ Correspondence to: xqing@hsc.pku.edu.cn.

SUMMARY

Cancer develops through a gradual accumulation of mutations including nonsense mutations in tumor suppressor genes (TSGs), which drive tumor proliferation and progression due to the impairment or complete loss of tumor suppressor protein function. The ability to restore functional tumor suppressor protein from mutant driver TSGs is a longstanding aspiration in cancer therapy, however, current strategies face formidable challenges in recovering proteins harboring heterogeneous mutations and circumventing dominant-negative effects exerted by endogenous mutant proteins. Therefore, the development of therapeutic interventions that are effective and generalizable across diverse nonsense mutations in cancer, to rescue endogenous mutant tumor suppressor proteins remains an urgent yet unmet need. Here we find that engineered suppressor transfer RNA (sup-tRNA) could overcome nonsense mutations in key driver tumor suppressor genes, such as *TP53*, thereby avoiding the dominant-negative effects through the restoration of endogenous mutant p53 with its original functions. Optimized sup-tRNA that we named super tRNA, enabling high-fidelity incorporation of desired amino acids, can further enhanced the transcriptional activity of p53 to suppress tumor cell proliferation. Moreover, we also establish a computational model to guide super tRNAs design, and demonstrate that super tRNA could effectively inhibit tumor growth by targeted readthrough of nonsense mutations in different tumor suppressor genes. In two xenograft models harboring nonsense mutant *TP53*, we observed up to a 70% reduction in tumor volume after lipid nanoparticle (LNP)-based sup-tRNA treatment, along with robust recovery of p53 expression and function, and no hematological or histological abnormalities detected. Our findings demonstrate the potential of sup-tRNA as a feasible and effective strategy to rescue and enhance tumor suppressor protein function, thereby preventing cancer development. As a novel therapeutic RNA, sup-tRNA provides a flexible strategy for targeting driver mutations in cancer, thereby expanding the

potential of tRNA-based therapy in precision oncology.

INTRODUCTION

Cancer is a disease of uncontrolled proliferation by transformed cells harboring mutations in driver genes including tumor suppressor genes and oncogenes[1-3]. Notably, over half of the high frequency mutations occur in tumor suppressor genes[4,5], like *TP53*, mutations of which are found in approximately 42% of patients worldwide and their pivotal role in cancer development has been well established[6,7]. According to global cancer statistics reported by WHO, approximately 1 million new cancer cases annually harbor *TP53* nonsense mutations, leading to truncated inactive p53 proteins or complete loss of expression due to nonsense-mediated mRNA decay[8,9] (NMD). However, rescuing these mutations remains a significant challenge in current therapies[10]. Unlike targeting mutations in oncogenes by inhibiting or degrading aberrant oncoproteins directly, rescuing tumor suppressor gene mutations requires the restoration of functional tumor suppressor proteins, which poses a formidable challenge to bind and recover mutant proteins of heterogeneous inactivating mechanisms with a single agent[11-13]. Large-scale studies have identified potential drug molecules, such as Rezatapopt and arsenic trioxide (ATO), which could stabilize p53 mutants and restore their functional conformation, through inserting into the Y220C crevice[14] or filling the arsenic-binding pocket in p53 proteins, respectively[15-17]. However, their efficacy is clearly limited to p53 mutants with these specific binding sites and is not applicable for rescuing other *TP53* mutations, particularly nonsense mutations[11,18].

As nonsense mutations result in premature termination of p53 translation, a facile and promising strategy is to restore endogenous full-length p53 by translational readthrough of nonsense codons during protein synthesis, avoiding undesirable adverse effects associated with exogenous p53

overexpression and the dominant-negative effects of truncated mutant proteins often observed in conventional gene therapy. In this context, developing therapeutic agents capable of recognizing and overriding only three nonsense codons (UAG, UAA, UGA) could address diverse *TP53* nonsense mutants, sparking renewed enthusiasm in recent years. To date, a few lead compounds, including aminoglycoside antibiotics and nucleoside analogs, have shown potential in overcoming cancer-derived *TP53* nonsense mutations and inhibiting tumor growth[19-22]. However, the reported readthrough approaches have yet to meet clinical needs, primarily due to their low efficiency (<10%) in most cases and the non-specific insertion of random amino acids in response to nonsense mutations, which may lead to the restoration of deleterious missense p53 mutants[23].

Suppressor tRNA (sup-tRNA), derived from natural transfer RNAs, could recognize and pair with the nonsense codon during translation elongation, thus restoring the production and function of the full-length protein[24-26]. Given the high efficiency, low toxicity, and minimal safety concerns associated with sup-tRNA in treating inherited diseases caused by nonsense mutations, we anticipate that it also holds great promise for addressing nonsense mutations in human cancer. With this inspiration, we hypothesized that sup-tRNA can be used to restore p53 from nonsense mutations and induce tumor regression. Drawing from prior knowledge of p53 mutations, we further set out to established the framework to optimize sup-tRNA for rescuing diverse nonsense mutant p53 variants.

93 **RESULTS**

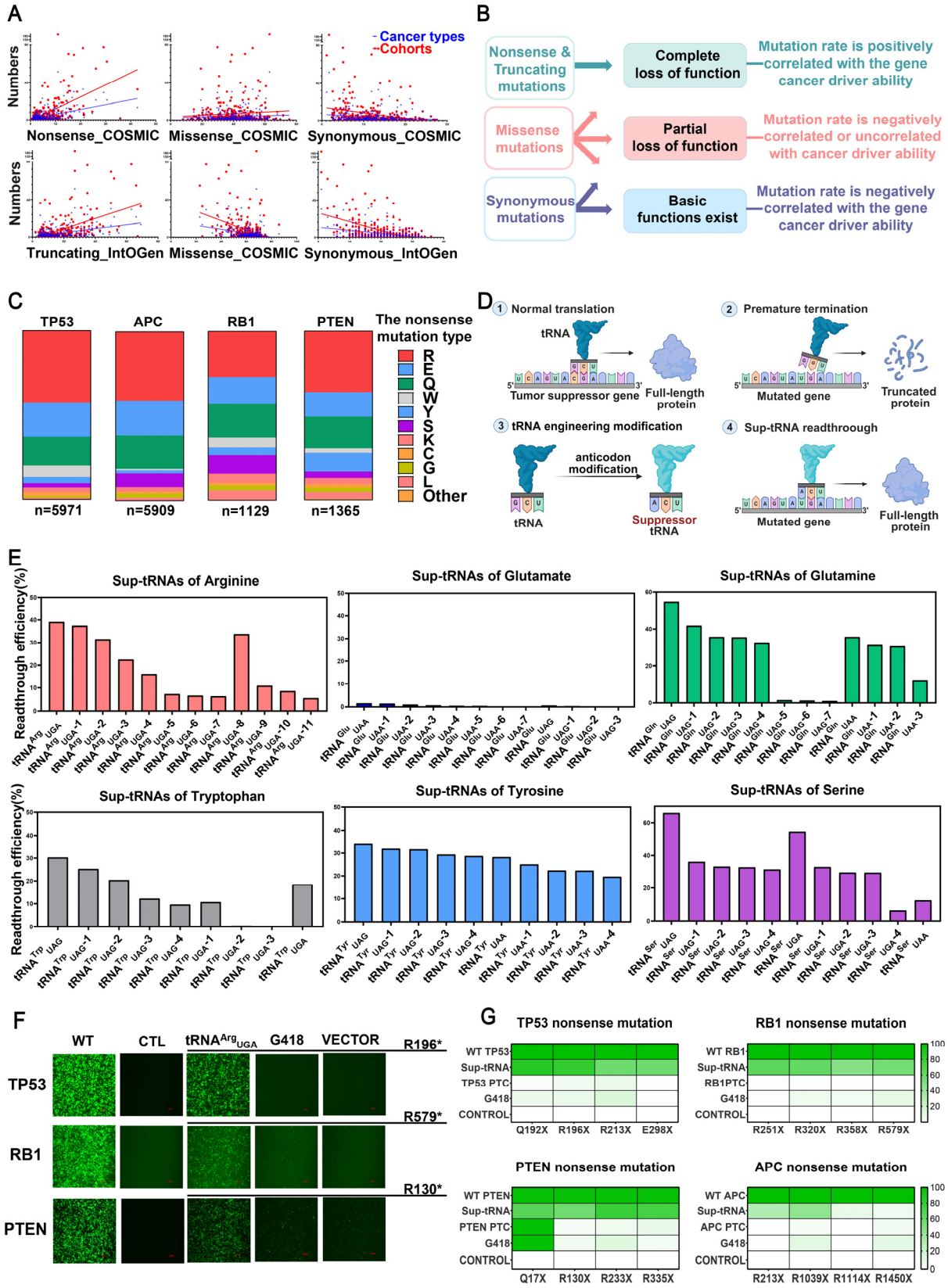

94

95 **Figure 1. The efficacy of sup-tRNA in overcoming nonsense mutations within tumor suppressor**

96 **genes**

(A) Scatter plots of the proportion of mutation types（nonsense/ truncating mutation, missense mutation, synonymous mutation）and the number of cancer types and cohorts which specific tumor suppressor genes act as driver genes in the Catalogue of Somatic Mutations in Cancer (COSMIC) and Integrative OncoGenomics (IntOGen) for mutational cancer driver tumor suppressor genes.

(B)The hypothesis explaining the correlation between the proportion of driver tumor suppressor genes mutation types and the cancer driver ability (In how many types of cancer/cohorts it serves as a driver gene). Based on the existing theories, nonsense mutation most leads to the complete loss of function thus missense mutation may cause complete loss of function or partial loss of function. The synonymous mutation leads to a partial loss of function or basic function. The variability in different mutation fates can rationally explain the correlation described above.

(C) Classification of nonsense mutations according to their original codons and corresponding amino acids, and statistics of the mutation rates in tumor suppressor genes including *TP53*, *APC*, *RB1*, and *PTEN*, based on data adapted from COSMIC.

(D) Schematics of engineering natural transfer RNA (tRNA) to suppressor tRNA (sup-tRNA) for nonsense mutations readthrough in tumor suppressor transcripts.

(E) Quantification of readthrough efficiency of sup-tRNA encoding highly mutated amino acid defined in (C) using the dual-luciferase reporter assay.

(F and G) Microscopy images (F) and quantification (G) of GFP positive cells showing differential readthrough efficiencies of above three approaches. Consistent results were obtained independently for at least three biological replicates. In (F and G), all data shown from HEK 293T cell experiments are mean of three biological replicates. Scale bar=100 μm.

Engineering sup-tRNAs to target nonsense mutations in *TP53*

Tumor suppressor genes often harbor nonsense mutations, which cause abnormal termination of the translation of tumor suppressor proteins, thereby driving the development of tumors. For different tumor suppressor genes, the proportion of nonsense mutations in the total mutations varies greatly. We found that certain tumor suppressor genes (such as *TP53*, *RB1*, *PTEN*, and *APC*) often have a relatively high proportion of nonsense mutations. Furthermore, we quantify the "driver ability" of tumor suppressor genes according to the number of cancer types/cohorts in which this gene functions as a cancer driver gene. *TP53* is regarded as the gene with the strongest driver ability, as it exists as a mutational cancer driver gene in more than 50 types of cancer. Interestingly, our analysis of 315 driver tumor suppressor genes[2] revealed a striking correlation: genes with higher driver ability exhibit a significantly higher proportion of nonsense/truncating mutations ($p < 0.001$), whereas synonymous mutations show an inverse trend (Figures 1A and S1A). This suggests that

133 nonsense mutations, causing disastrous protein function loss, are evolutionarily
134 selected in key tumor suppressors to promote tumor initiation (Figures 1B and
135 S1-S2).
136
137 We then analyzed the types of amino acids affected by nonsense mutations in
138 the four vital tumor suppressor genes *TP53*, *APC*, *RB1*, and *PTEN*. The amino
139 acids involved in these mutations were similar across these genes, primarily
140 consisting of arginine (Arg), glutamic acid (Glu), and glutamine (Gln) (Figure
141 1C). With the exception of glutamic acid, all frequently mutated amino acids had
142 corresponding suppressor tRNAs capable of inducing nonsense readthrough
143 by up to 55%, offering potential for the restoration of tumor suppressor proteins
144 (Figures 1D-1E). Next, we constructed a series of surrogate reporters harboring
145 nonsense mutant tumor suppressor genes and EGFP genes linked by a 2A
146 peptide sequence, and employed sup-tRNAs to induce targeted readthrough of
147 nonsense codons (UAG, UGA) to permit the downstream enhanced green
148 fluorescent protein (EGFP) expression, allowing us to measure the readthrough
149 efficiency through monitoring EGFP level. Though readthrough efficiency varies
150 among different genes, we found that sup-tRNA consistently outperforms the
151 documented readthrough-promoting agent G418 (geneticin), achieving up to a
152 276-folds increase in efficiency (Figures 1F-1G). These results indicate that
153 sup-tRNA can efficiently overcome nonsense mutations in tumor suppressor
154 genes, inducing nearly 70% readthrough in nonsense mutant *TP53*. The actual
155 amino acids incorporated by these sup-tRNAs have been verified by mass
156 spectrometry. These results suggested that sup-tRNA enabled the efficient and
157 precise incorporation of specific amino acids at nonsense mutations.
158
159 To further investigate the capability of sup-tRNAs for the functional restoration
160 of p53, we co-transfected NCI-H1299 cells (*TP53*-null) with sup-tRNAs, the p53
161 reporter, and a genetically encoded sensor, which allowed us to characterize
162 full-length p53 protein expression via green fluorescence and assess its

163 transcriptional activity restoration through red fluorescence (Figure 2A). We
164 found that sup-tRNAs carrying glutamine or arginine were able to rescue the
165 expression and function of the frequent p53 mutants, albeit with varying
166 efficiencies (Figures 2B-2C and S3-S5). Furthermore, functional restoration
167 exhibited a significant correlation with readthrough efficiency. However, when
168 applying the high-efficiency sup-tRNAs to address other COSMIC-reported p53
169 mutants harboring UAG or UGA nonsense mutations, we observed that the
170 function of two mutants (G266* and Y234*) was not restored, despite the
171 recovery of full-length protein expression (Figures 2B and S4). By analyzing
172 Y234* and G266* variants based on p53 crystal structure with molecular
173 dynamics simulation, we speculated that mischarging of Y234Q and G266R in
174 p53, induced by sup-$tRNA^{Gln}_{UAG}$ and sup-$tRNA^{Arg}_{UGA}$, may be deleterious
175 (Figure 2E). This is primarily attributed to the disruption of a hydrophobic core
176 around Y234 and the formation of new hydrogen bonds between G266 and
177 adjacent residues, potentially compromising the p53-DNA binding interface
178 (Figure 2E). Therefore, a reliable approach for restoring p53 activity
179 necessitates the simultaneous consideration of readthrough efficiency and the
180 functional impact of the incorporated amino acid.

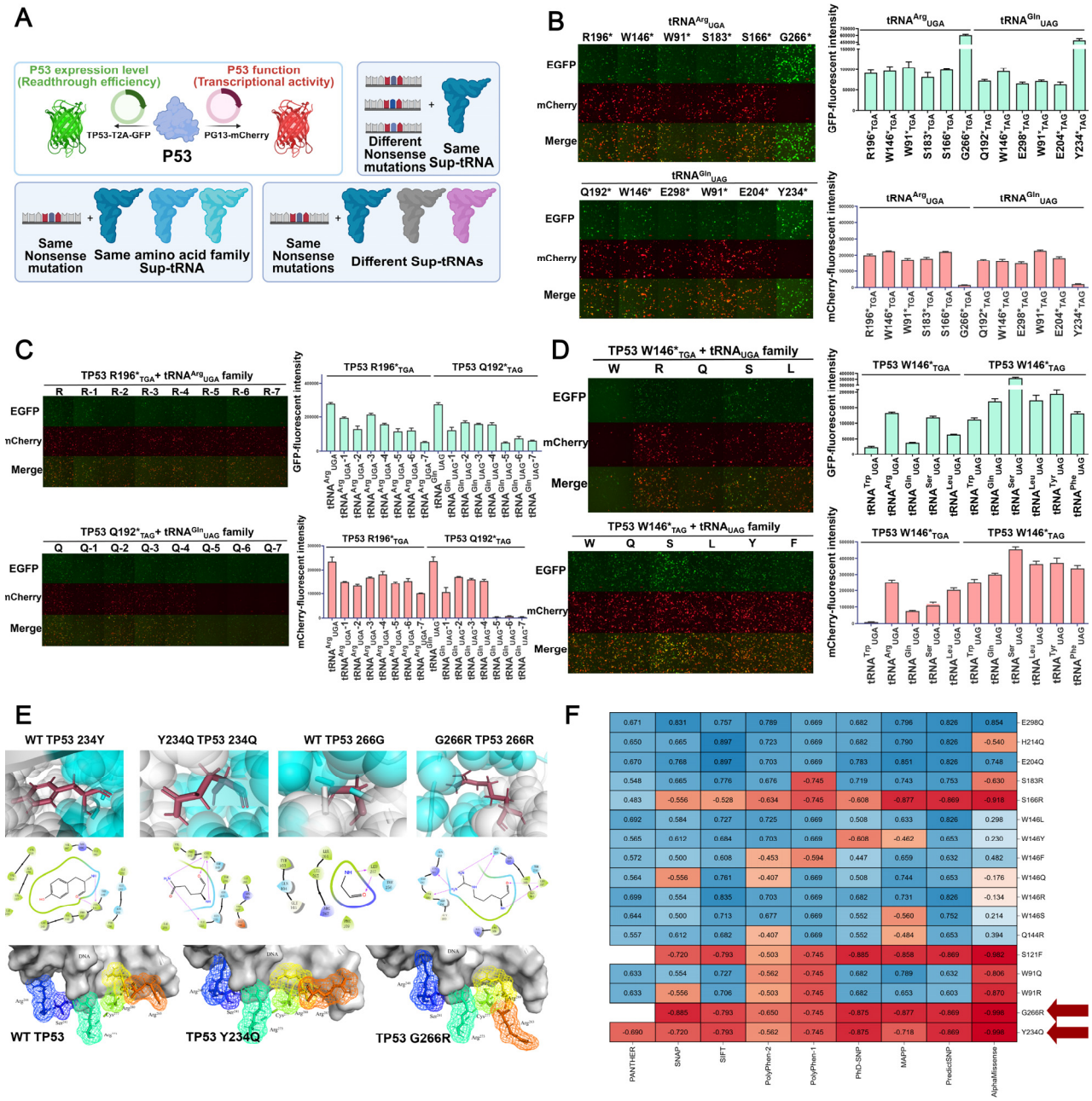

Figure 2. Characterization of sup-tRNA in recovering p53 expression and function

(A) Schematic of a genetically encoded reporter system to measure the expression and function of p53 via dual-fluorescence detection, which is designed for sup-tRNA efficiency characterization.

(B) Representative microscopy images (left) and quantification of GFP and mCherry positive cells (right) show p53 expression and function in NCI-H1299 cells with 12 kinds of nonsense mutations after $tRNA^{Arg}_{UGA}$ and $tRNA^{Gln}_{UAG}$ readthrough. Data are mean ± s.d. of three biological replicates. Scale bars = 100 μm.

(C) Representative microscopy images (left) and quantification of GFP and mCherry positive cells (right) show p53 expression and function in NCI-H1299 cells with *TP53* R196*& *TP53* Q192* nonsense mutations after 8 kinds of arginine (R) and 8 kinds of glutamine (Q) sup-tRNAs readthrough. Data are mean ± s.d. of three biological replicates. Scale bars = 100 μm.

(D) Representative microscopy images (left) and quantification of GFP and mCherry positive cells (right) show p53 expression and function in NCI-H1299 cells with *TP53* W146* nonsense mutations after 7 amino

acids while 12 kinds of high-efficiency sup-tRNAs readthrough. Data are mean of three biological replicates. Scale bars = 100 μm.

(E) Verified deleterious p53 variants mutant site amino acid residues and intermolecular forces. The first and third panels show the 234Y, and 266G structures of wild-type (WT) p53 DBD (2AC0), respectively. The other panels are drawn by mutating 234Y, 266G residue in wild-type DBD (2AC0) into the indicated residues in PyMOL and Schröder. The panels below show the close-up view of the wild-type and verified deleterious p53 DNA binding peptides and DNA. The side chains of the six classic DNA binding residues are shown as sticks.

(F) Predictive and functional profile of p53 previous variants. The heat map corresponds to the predictive impact of each p53 variant ranging from -1 (red) to 1 (blue), with the lowest score being the most deleterious. Scores from the 9 algorithms in the panels including AlphaMissense, MAPP, PANTHER, PhD-SNP, PolyPhen-1, PolyPhen-2, SIFT, and SNAP. Red arrows indicate previous verified deleterious p53 variants.

Computationally optimized screening of sup-tRNAs for enhanced p53 activity restoration

To this end, we developed a computational tool[27,28] to predict the functional impact of incorporated amino acids, facilitating the selection of optimal sup-tRNAs (Figure 2F). Using the p53-E204* mutant cancer cell line containing a TAG codon, we assessed its expression and functional restoration following readthrough induced by sup-tRNAs carrying different amino acids (Figure S7A). Consistent with the prediction, we found that $tRNA^{Tyr}_{UGA}$, $tRNA^{Phe}_{UGA}$, and $tRNA^{Trp}_{UGA}$ failed to restore p53 transactivation function due to the insertion of undesired amino acids, despite its high readthrough efficiencies (Figure S7B). Moreover, even when the original amino acid could not be restored due to the low readthrough efficiency of the corresponding $tRNA^{Glu}_{UGA}$, high-efficiency sup-tRNAs, such as $tRNA^{Gln}_{UGA}$ and $tRNA^{Ser}_{UGA}$, served as effective alternatives to rescue p53 function, provided that the incorporated amino acid, as predicted, does not disrupt the protein structure (Figure S8-S9). Further investigation also confirmed the robustness of this alternative strategy in restoring other functional p53 mutants, however, we noticed that some recovered p53 variants showed superior transcriptional activity compared to wild-type p53 proteins, for instance, $tRNA^{Arg}_{UGA}$ outperformed $tRNA^{Trp}_{UGA}$ in functional restoration of p53-W146*$_{TGA}$ mutant (Figure 2D), even though the

228 latter enabled recovery of wild-type p53 proteins.

229

230 These observations can be mechanistically explained by two critical
231 determinants governing p53 functional restoration. First, when the incorporated
232 amino acid induces minimal structural perturbation to native conformation of
233 p53, sup-tRNAs with higher readthrough efficiency, such as $tRNA^{Gln}_{UAG}$, sup-
234 $tRNA^{Arg}_{UGA}$, can achieve superior functional restoration (Figures 2B-2D and S4-
235 S6). Second, in cases where readthrough efficiencies are comparable across
236 different sup-tRNAs, the identity of the restored amino acid becomes
237 particularly crucial.

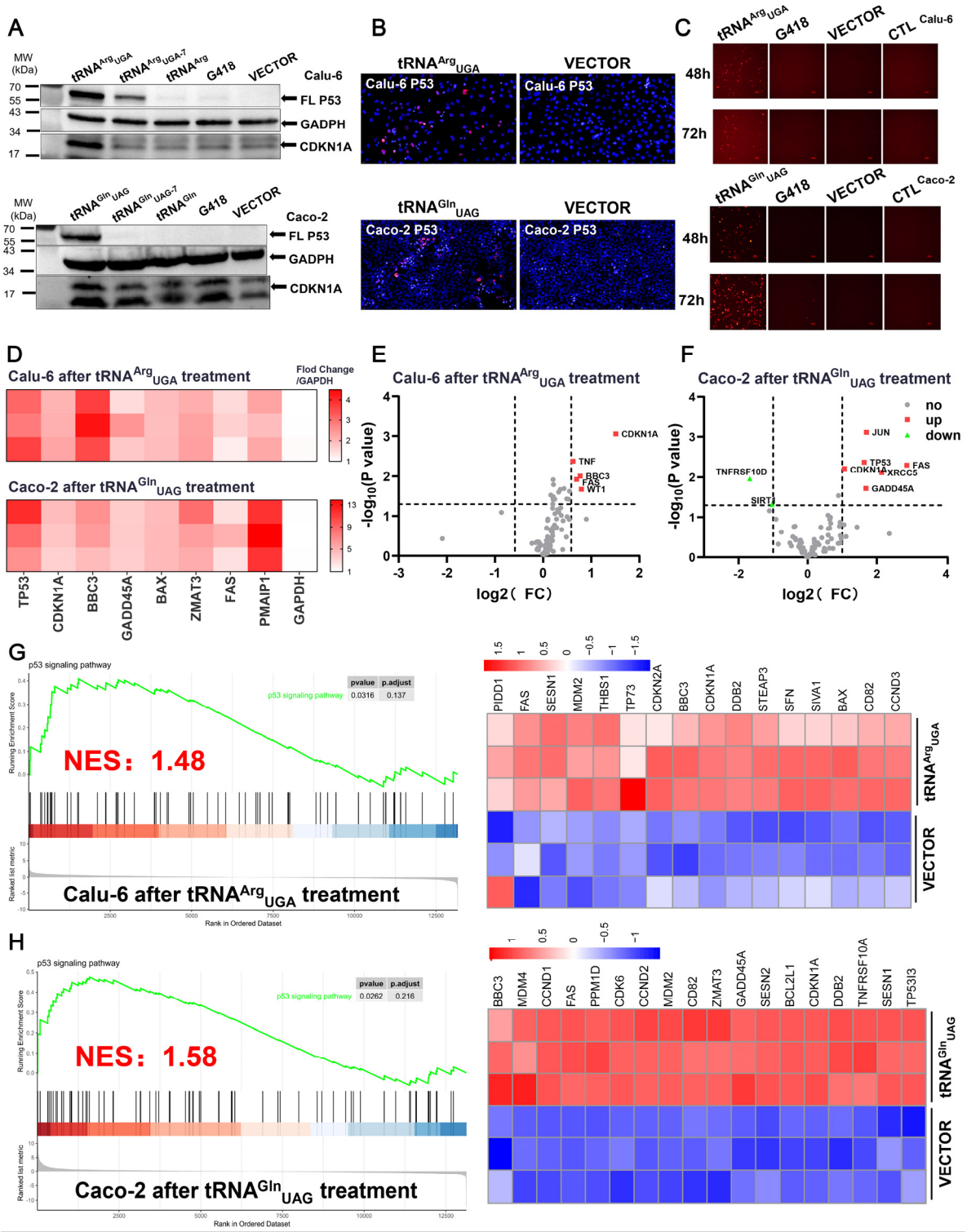

Figure 3. Sup-tRNA rescues endogenous full-length p53 expression and restores its transcriptional activity

(A) Western blot analysis of full-length p53 recovery and protein expression from its target gene *CDKN1A* in Calu-6 (above) & Caco-2 cells (below) treated with sup-tRNA, corresponding tRNA, vector, and G418 for 48 hours, respectively.

(B) Representative microscopy images of immunofluorescence for full-length p53 and CDKN1A in Calu-6 (above) & Caco-2 cells (below) treated with sup-tRNA or vector for 48h. Scale bars= 20 μm. Data shown

here were representative examples from n=3 independent biological replicates.
(C) Representative microscopy images showing the transcriptional activity of endogenous p53 in Calu-6 (above) & Caco-2 cells (below). treated with sup-tRNA, corresponding tRNA, vector, and G418 for 48&72 hours Data shown here were representative examples from n=3 independent biological replicates.
(D) Quantification of mRNA levels of *TP53* and its target genes *CDKN1A*, *BBC3*, *GADD45A*, *BAX*, *ZMAT3*, *FAS*, and *PMAIP1* after sup-tRNA treatment in Calu-6 (above) & Caco-2 cells (below) for 48h by qRT-PCR. All the mRNA expression levels are normalized to *GAPDH*. Data are represented as mean for n = 3 independent biological replicates.
(E and F) Significant differential expressed of p53-relatived transcripts are determined by p53 PCR array on Calu-6 (E) & Caco-2 (F) treated with sup-tRNA, or vector control, n = 3.
(G and H) Gene Set Enrichment Analysis (left) and gene expression analysis (right) of p53 signaling pathways on Calu-6 (G) & Caco-2 cells (H) treated with sup-tRNA, or vector control, n = 3.

Harnessing sup-tRNAs to overcome endogenous *TP53* nonsense mutations

Genomic analyses from COSMIC and intOGen databases have consistently identified *TP53* nonsense mutations as one of the most prevalent genetic alterations in non-small cell lung carcinoma (NSCLC) and colorectal cancer (CRC) (Figures S10A-S10B). TCGA data further highlight *TP53* as the most critical driver gene in both NSCLC and CRC (Figures S10C-S10D). Therefore, we further investigated the efficacy of sup-tRNAs using NSCLC cell line Calu-6 (*TP53* R196*$_{TGA}$) and CRC cell line Caco-2 (*TP53* E204*$_{TAG}$), whose nonsense mutant *TP53* genes have been verified by whole-genome sequencing (Figures S10E-S10F). In Calu-6 cells, tRNA$^{Arg}_{UGA}$, engineered from an arginine-carrying tRNA with a UCU anticodon, effectively restored high levels of full-length p53 expression (Figure 3A). In contrast, G418 treatment resulted in only minimal p53 recovery, comparable to the tRNA$^{Arg}_{UGA}$ control and even significantly lower than that achieved with the low-efficiency (~6%) tRNA$^{Arg}_{UGA}$-7 (Figure 3A). In Caco-2 cells, tRNA$^{Gln}_{UAG}$ also yielded a robust restoration of full-length p53 protein expression compared to other groups, as determined by western blot analysis (Figure 3A). The recovery of p53 transactivation function was confirmed by red fluorescent encoded by the sensor (Figures 3C and S11) and increased expression of cyclin-dependent kinase inhibitor 1A (CDKN1A), a major downstream target of p53 activity, and the recovery of p53 expression

279 further validated through immunostaining (Figures 3A-3B).

280

281 Classically, p53 functions mainly as a sequence-specific transcription factor that
282 can bind to p53 response element and activate the transcription of target genes.
283 To evaluate the transcriptional activity of restored p53, we examined the
284 expression levels of its target genes using RT-qPCR. Our results showed that
285 the RNA expression levels of p53 and its downstream targets were upregulated
286 to varying degrees in both Calu-6 and Caco-2 cell lines (Figure 3D). Notably,
287 the extent of upregulation increased over time, suggesting that sup-tRNA may
288 prevent *TP53* mRNA with nonsense mutations from degradation by nonsense-
289 mediated mRNA decay[9] (NMD), thereby promoting full-length p53 production
290 for transactivation. To further confirm the efficacy of sup-tRNA in reactivating
291 p53-related genes, we performed a PCR array analysis. In Calu-6 cells, RNA
292 expression levels of p53 target genes, including *CDKN1A* and *BBC3*, were
293 differentially upregulated following readthrough restoration of p53 (Figure 3E).
294 Similarly, in Caco-2 cells, RNA expression levels of *TP53* and its downstream
295 targets were differentially upregulated, which consistent with RT-qPCR results
296 (Figure 3F).

297

298 Moreover, RNA-seq analysis enabled us to assess the global influence of sup-
299 tRNA on the transcriptomes of Caco-2 and Calu-6 cells. Gene Set Enrichment
300 Analysis (GSEA) revealed that, compared with the control group, sup-tRNA
301 treatment significantly upregulated the p53 signaling pathway in tumor cells
302 from both Calu-6 (NES = 1.48, $p = 0.0316$) and Caco-2 (NES = 1.58, $p = 0.0262$)
303 (Figures 3G-3H). The mRNA expression of p53-target genes also showed a
304 significant increase compared to the control group (Figures 3G-3H).

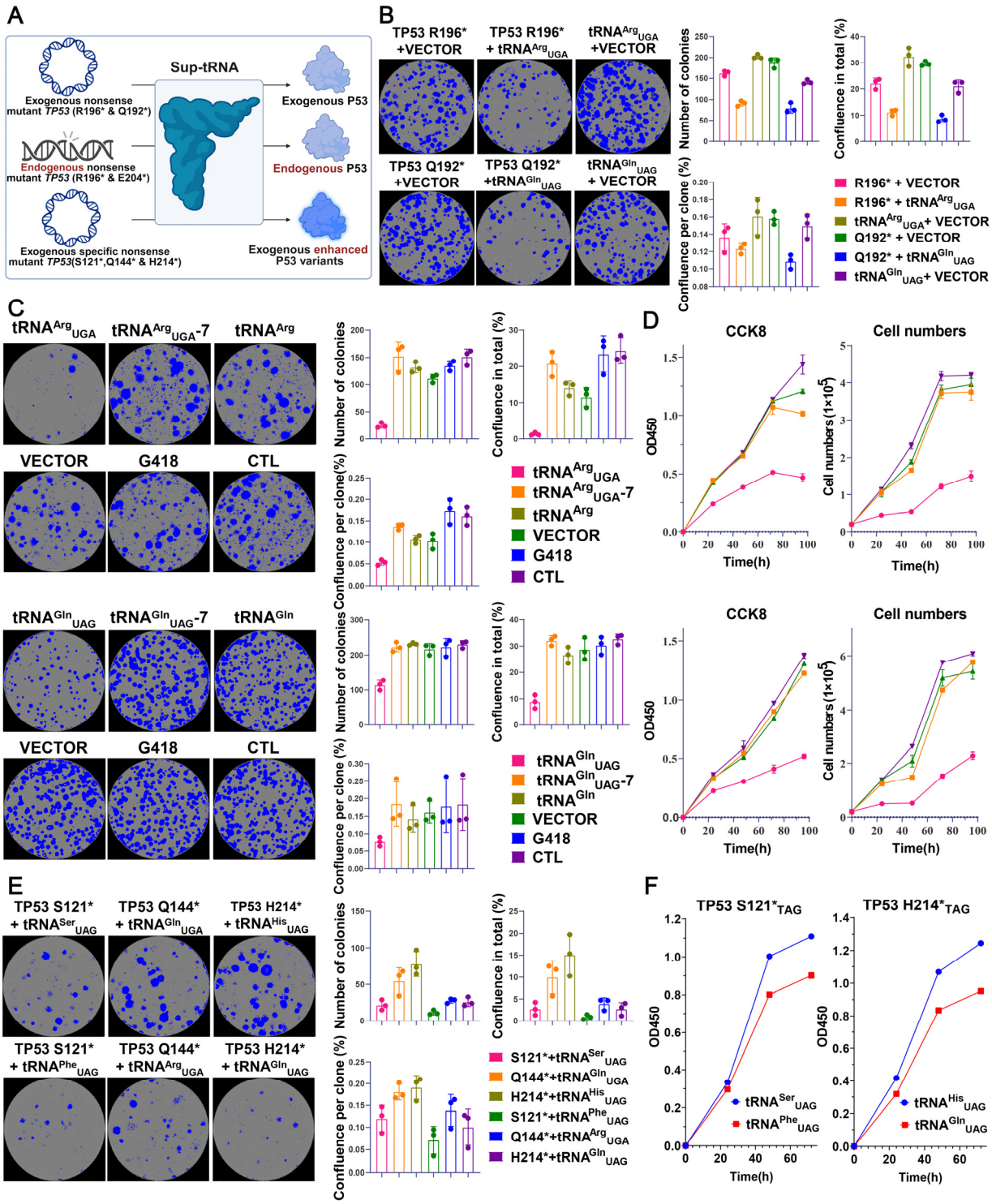

Figure 4. Sup-tRNA elicits antiproliferation activity through p53 restoration

(A) Schematic workflow for measure antiproliferative effects mediated by p53 restoration via sup-tRNA readthrough.

(B) Sup-tRNAs in the presence of *TP53* exogenous nonsense mutation reduces the colony formation in human NCI-H1299 cells. Colonies are stained with crystal violet staining solution and counted after 10-12 days of culture. Colony images are acquired by Incucyte SX5 and processed and analyzed by Incucyte 2022B Rev2. Data are represented as mean ± SEM, n = 3.

(C) Sup-tRNA treatment reduce the colony formation in human Calu-6 (above) & Caco-2 (below) cell which

have genomic *TP53* nonsense mutation. Colonies are stained with crystal violet staining solution and counted after 10-12 days of culture. Colony images are acquired by Incucyte SX5 and processed and analyzed by Incucyte 2022B Rev2. Data are represented as mean ± SEM, n = 3.

(D) Cell proliferation curve was measured by CCK-8 (left) and cell count assay (right). After transfecting human Calu-6 (above) & Caco-2 (below) cell for 8 hours, the cells are digested, spread in plates and further measured. Data are represented as mean ± SEM, n = 3.

(E) The superb-tRNA strategy compared to the strategy restore as wild-type p53 reduces the colony formation in human NCI-H1299 cell which introduce exogenous *TP53* nonsense mutation. Colony images are acquired by Incucyte SX5 and processed and analyzed by Incucyte 2022B Rev2. Data are represented as mean ± SEM. N = 3.

(F) CCK8 shows the superb-tRNA strategy compared to the strategy restore as wild-type p53 had a stronger growth inhibitory effect on the human NCI-H1299 cell which introduces exogenous *TP53* nonsense mutation.

Suppressing tumor cell proliferation by restoring p53 function

To verify that sup-tRNA could inhibit tumor cell growth by suppressing nonsense mutations in the *TP53* gene, we transfected *TP53*-null NCI-H1299 cells with both a nonsense mutant *TP53* and sup-tRNA, or with either component individually (Figure 4A). The colony formation assay demonstrated that sup-tRNA exerted tumor-suppressive effects only in the presence of *TP53* nonsense mutations readthrough, leading to approximately a 60% reduction in colony number, a 70% decrease in total colony area, and a 30% reduction in the average area of individual clones (Figure 4B). In contrast, sup-tRNA alone did not exhibit significant proliferation-inhibitory effects in tumor cell lines lacking nonsense mutant *TP53* (Figure 4B).

Next, we sought to evaluate the efficacy of sup-tRNA in suppressing the proliferation of tumor cells harboring endogenous *TP53* nonsense mutations. Treatment with high-efficiency sup-tRNAs resulted in significant inhibition of cell growth and reduced cell viability. In Calu-6 cells, restoration of p53 using $tRNA^{Arg}_{UGA}$ resulted in a notable reduction in colony number, total colony area, and individual clone size, outperforming both G418 treatment and the low-efficiency control, consistent with previous findings (Figures 4C-4D). Similar results were also observed in Caco-2 cells, further highlighting the robustness

347 of sup-tRNA across different cell lines (Figures 4C-4D). Given that nonsense
348 mutant *TP53* could produce missense p53 variants with enhanced tumor
349 suppressor function[29] via sup-tRNA-mediated readthrough (Figure 4A), we
350 further demonstrated the augmented efficacy of restored p53 variants S121F,
351 Q144R, H214Q in inhibiting tumor cell growth (Figures 4E-F and S12-S13). As
352 conventional gene therapy could only introduce wild-type p53 that may be
353 neutralized by endogenous truncated p53 in a dominant-negative effect[30], high-
354 efficiency sup-tRNAs could directly convert truncated p53 into functional p53
355 variants[29](Figure S14) in suppressing tumor cell proliferation, providing a
356 plausible strategy for cancer therapy.

357 **Super- and superb-tRNA strategies for tRNA therapy**

358 By applying first principles thinking, we have delineated tRNA therapy into two
359 determinants: (1) Efficient restoration of full-length protein expression, which is
360 governed by the readthrough efficiency of the specific sup-tRNA. (2) Functional
361 recovery of restored protein, influenced by properties of the incorporated amino
362 acid at nonsense mutations. Therefore, the most straightforward strategy for
363 tRNA therapy is to restore original amino acids at nonsense mutations, which is
364 particularly applicable to arginine and glutamine mutations, due to the high
365 efficiency of $tRNA^{Arg}_{UGA}$ and $tRNA^{Gln}_{UAG}$ (Figure 1E). However, this strategy
366 cannot facilitate the readthrough of approximately 43% nonsense mutations in
367 *TP53*, since the low efficiency of corresponding sup-tRNAs. Thus, we reasoned
368 that an alternative is using high efficiency sup-tRNA to convert the nonsense
369 mutation to a missense but neutral mutation in proteins, based on
370 computational analysis, which is named as super-tRNA therapy (Figure S15A).
371 Meanwhile, we defined the strategy of converting nonsense mutations into wild-
372 type proteins through high efficiency sup-tRNAs, which was previously used in
373 treating inherited diseases, as primary-sup-tRNA therapy. Conversely, utilizing
374 sup-tRNAs to restore deficient protein expression, or to cause missense and
375 deleterious mutations, called lower-sup-tRNA therapy, ought to be avoided in

376 future applications (Figure S15A).

377

378 Aforementioned results suggested the feasibility of super-tRNA in multiple
379 aspects. For *TP53* W146*$_{TGA,}$ although both tRNA$^{Trp}_{UGA}$ and tRNA$^{Arg}_{UGA}$ could
380 suppress this nonsense mutation, tRNA$^{Arg}_{UGA}$, increased the restored protein
381 expression level by 5.7 folds and the transcriptional function by 27 folds,
382 compared with tRNA$^{Trp}_{UGA}$. Similarly, for *TP53* W146*$_{TAG}$, tRNA$^{Ser}_{UAG}$
383 outperformed tRNA$^{Trp}_{UAG}$, in increasing the restored protein expression level by
384 3.2 folds and the transcriptional function by 1.8 folds (Figure 2D). It is worth
385 noting that super-tRNA is engineered for restoring nonsense mutations to
386 neutral mutations, but not for restoring them to deleterious missense mutations.
387 For example, we attempted to restore *TP53* G266*$_{TGA}$ and Y234*$_{TAG}$ using
388 tRNA$^{Arg}_{UGA}$ and tRNA$^{Gln}_{UAG}$ respectively. The efficient restoration of protein
389 expression was achieved by both sup-tRNAs, but neither could rescue protein
390 functions. We attribute this to the restoration of the *TP53* G266R and Y234Q
391 mutations, which are considered deleterious mutations (Figures 2B and S4).
392 Surprisingly, all these deleterious mutations can be accurately identified by the
393 computational tools, which indicates that super-tRNA therapy can be safely
394 applied with the assistance of the computational tools. These results suggest
395 that a single super-tRNA could be employed to treat 10 different amino acid
396 types of nonsense mutations, which would significantly reduce the cost in
397 developing drug development (Figures 2F and S15B).

398

399 In addition to recovery of wild-type or neutral p53 variants, we anticipated that
400 sup-tRNA could produce p53 with enhanced functions, via high-fidelity specific
401 amino acid incorporation at nonsense mutations (Figure S15A). Some p53
402 variants, including S121F, H214Q, and Q144R, have been shown to exhibit
403 enhanced apoptotic induction compared to wild-type p53, suggesting that
404 enhancing p53 function would contribute to tumor inhibition [29]. Here we termed
405 this sup-tRNA based strategy as superb-tRNA strategy (Figure 15A) and

406 attempted to restore *TP53* S121*, H214*, and Q144* to produce advantageous
407 p53 variants with enhanced anti-cancer function (Figure 4A). The superb-tRNA
408 strategy achieved more efficient tumor suppression effects at all the three
409 aforementioned nonsense mutations. Compared with restoration of wild-type
410 p53, all advantageous p53 variants achieved more pronounced tumor
411 suppression, resulting in up to 80% reduction in colony number and 90%
412 reduction in total colony area (Figures 4E-4F), which is consistent with previous
413 reports[29].
414
415 Therefore, by leveraging the capacity of tRNAs to precisely incorporate desired
416 amino acids during protein translation, we could restore p53 variants with
417 retained (super-tRNA therapy) or even enhanced functions (superb-tRNA
418 strategy), supported by computational guided sup-tRNA selection (Figures 2F
419 and S15). We also noted that a recent investigation employed CRISPR-
420 mediated homology-directed repair to engineer 9,225 p53 variants in cancer
421 cells, covering over 94% of cancer-associated missense mutations, and
422 mapped their effects on p53 function[31]. These precious data are also helpful for
423 choosing specific sup-tRNA for super-tRNA and superb-tRNA therapy .

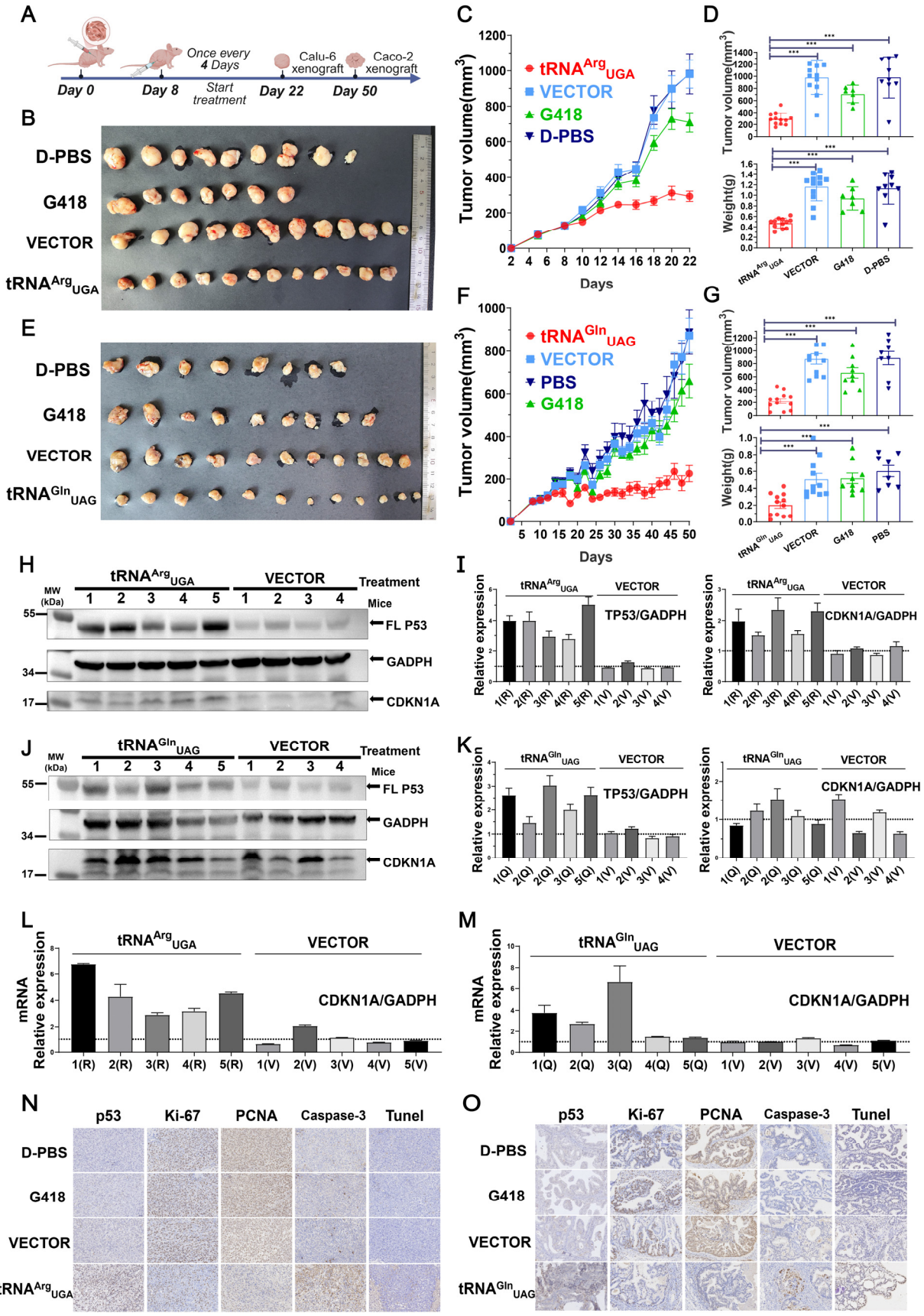

Figure 5. Therapeutic efficacy of sup-tRNA therapy *in vivo*

(A) Schematic of therapeutic evaluation of sup-tRNA therapy.

427 (B) Images of Calu-6 xenograft excised tumors.
428 (C and D) Tumor growth curves (C), volumes (above) and weights(below) of tumor collected on Day 22
429 (D) in Calu-6 xenograft model after $tRNA^{Arg}_{UGA}$ treatment. *P*-values were calculated by one-sided t test.
430 (E) Images of Caco-2 xenograft excised tumors.
431 (F and G) Tumor growth curves (F), volumes (above) and weights(below) of tumor collected on Day 50
432 (G) in Caco-2 xenograft model after $tRNA^{Gln}_{UAG}$ treatment. *P*-values were calculated by one-sided t test.
433 (H and I) Western blot analysis of full-length p53 recovery and protein expression of p53 target gene
434 *CDKN1A* in Calu-6 xenograft treated with sup-tRNA (H) and quantification of the expression of each
435 indicated protein relative to GAPDH expression, and normalized to the control mean (I). The abbreviation
436 for $tRNA^{Arg}_{UGA}$ is R, and the abbreviation for VECTOR is V. *P*-values were calculated by one-sided t test.
437 (J and K) Western blot analysis of full-length p53 recovery and protein expression of p53 target gene
438 *CDKN1A* in Caco-2 xenograft treated with sup-tRNA (J) and quantification of the expression of each
439 indicated protein relative to GAPDH expression, and normalized to the control mean (K). The abbreviation
440 for $tRNA^{Gln}_{UAG}$ is Q, and the abbreviation for VECTOR is V. *P*-values were calculated by one-sided t test.
441 (L and M) Quantification of mRNA levels of p53 target genes *CDKN1A* in Calu-6 (L) and Caco-2 (M)
442 xenograft by RT-PCR. All the mRNA expression levels are normalized to *GAPDH*. Data are represented
443 as mean ± SEM and individual data points shown for n = 3 independent biological replicates. *P*-values
444 were calculated by one-sided t test.
445 (N and O) Immunohistochemistry analysis of Calu-6 (O) and Caco-2 (P) xenograft including p53,
446 proliferation and apoptosis markers after corresponding treatments. Scale bar=50 μm. Data shown here
447 were representative examples from n=3 independent biological replicates.

448 ***In vivo* efficacy of sup-tRNA in *TP53* nonsense mutant xenograft**

449 Lipid nanoparticle (LNP)-based RNA therapy has emerged as a pioneering
450 platform in modern drug development. Its success in the COVID-19 pandemic
451 has validated its potential for rapid, scalable, and adaptable medical solutions.
452 As a novel therapeutic RNA, sup-tRNA can in theory be delivered to tumors via
453 LNP. Here we utilized classical FDA-approved LNP formulation in which SM-
454 102 serving as the ionizable lipid. All LNP-tRNAs (including $tRNA^{Arg}_{UGA}$ &
455 $tRNA^{Gln}_{UAG}$) formulations were monodisperse spherical nanoparticles with a
456 size of approximately 150 nm and possessed a slightly negative zeta potential
457 (Figure S16A-S16B), indicating that LNP-tRNA have a generally uniform
458 particle size distribution suitable for cellular uptake and endosomal escape,
459 thus facilitating cancer treatment *in vivo*.
460

461 We next utilized cell-line-derived xenograft (CDX) mouse models to investigate
462 whether sup-tRNA could restore p53 protein expression from *TP53* nonsense

463 mutations *in vivo* and inhibit tumor growth. Six-week-old immunodeficient nude
464 mice were implanted with either Calu-6 or Caco-2 cells to generate xenograft
465 models harboring *TP53* nonsense mutations, and were treated with LNP-tRNA
466 via intra-tumoral delivery once the tumor volume reached approximately 200
467 mm^3 (Figure 5A). For the NSCLC Calu-6 xenograft model with p53-R196*, we
468 treated the mice with LNP-$tRNA^{Arg}_{UGA}$ and G418 as a positive control. The
469 tumor growth curve of the LNP-$tRNA^{Arg}_{UGA}$ group showed a significantly slower
470 growth rate compared to the control groups after the first treatment (Day 8),
471 resulting in a tumor volume reduction of approximately 70% and no mortality by
472 the study endpoint (Day 22) (Figures 5C-5D and S17). In terms of functional
473 p53 recovery, sup-tRNA treatment resulted in a 3.7-fold increase in full-length
474 p53 expression and a 1.9-fold increase in downstream CDKN1A expression
475 compared to vector treatment (Figures 5I and S18A). RT-qPCR analysis also
476 revealed a 4.3-fold upregulation of *CDKN1A* transcripts in the sup-tRNA group
477 relative to vector (Figures 5L and S18A). Consistently, LNP-$tRNA^{Gln}_{UAG}$
478 treatment also significantly attenuated tumor progression in the CRC Caco-2
479 xenograft harboring p53-E204*, with no treatment-related mortality observed by
480 the endpoint (Day 50) (Figures 5E-5G and S17). Moreover, both protein levels
481 of p53 and the mRNA levels of *CDKN1A* were markedly elevated following sup-
482 tRNA treatment, whereas vector treatment showed minimal efficacy (Figures
483 5J-5M and S18B).
484
485 The tumor regression induced by p53 restoration is primarily attributed to p53-
486 mediated apoptosis and growth inhibition[32,33], as evidenced by a reduction in
487 Ki-67 and PCNA-positive proliferating cells, along with an increase in activated
488 caspase-3 and TUNEL-positive apoptotic cells in both xenograft models
489 following sup-tRNA treatment (Figures 5N-5O). Overall, these findings highlight
490 the robust efficacy and excellent safety profile of p53 restoration through sup-
491 tRNA-mediated translational readthrough, warranting further investigation into
492 its broader application in cancer therapy.

493 ***In vivo* potential toxicity of sup-tRNA**

494 Although aforementioned results showed that sup-tRNA alone did not inhibit
495 cell growth in the NCI-H1299 (*TP53*-null) cell line, only when co-transfection of
496 both sup-tRNA and *TP53* nonsense mutation gene led to growth inhibition
497 (Figure 4B). However, further investigations are needed to determine whether
498 the observed tumor regression is attributable to p53 restoration rather than
499 potential sup-tRNA toxicity.

500

501 Next, the potential toxicity of sup-tRNA *in vivo* was assessed in a mouse
502 xenograft model. Seven-week-old BALB/c mice were injected with an identical
503 number of *TP53*-null 4T1 cells (Figure S21A). According to previous reports[19-
504 22] , 4T1 and Calu-6 cells showed similar *in vivo* growth rates. Treatment of
505 *TP53*-null xenografts with LNP-tRNA, $tRNA^{Arg}_{UGA}$ or $tRNA^{Gln}_{UAG}$, could not
506 reduce tumor weight or volume by the study endpoint (Figures S21B-S21C),
507 and the tumor growth curves showed no significant difference compared to the
508 control group (Figure S21D). Moreover, no significant changes were observed
509 in p53, Ki-67 and PCNA-positive proliferating cells, along with activated
510 caspase-3 and TUNEL-positive apoptotic cells in each group (Figure S21F).
511 Consistently, we could not find significant perturbations in the p53 signaling
512 pathway after LNP-tRNA treatment (Figure S22). These results suggested that
513 sup-tRNA could induce tumor regression by restoring tumor suppressor
514 proteins, instead of its potential toxicity.

515

516 Furthermore, both in BALB/c nude mice and BALB/c mice, we did not observe
517 any toxicity induced by LNP-tRNA. Safety assessments demonstrated no
518 significant abnormalities in histopathological evidence of tissue damage
519 (Figures S19 and S23A) or hematological parameters (Figures S20 and S23B)
520 in sup-tRNA-treated mice, supporting the favorable therapeutic index of this
521 approach.

522 **DISCUSSION**

523 The distinct biological characteristics of oncogenes and tumor suppressor
524 genes pose fundamentally different challenges for therapeutic intervention. The
525 oncogene addiction in malignant tumors has a compelling therapeutic rationale
526 for the development of targeted therapies[34,35], such as kinase inhibitors[36] and
527 PROTACs[37], which aim to inhibit or degrade hyperactive proteins. In contrast,
528 tumor suppressor genes that often harbor loss-of-function mutations, typically
529 require functional protein restoration, posing a significant pharmacological
530 challenge[4,5]. Furthermore, mutant tumor suppressor proteins not only lose
531 tumor-suppressive functions, but can also actively antagonize reintroduced
532 wild-type proteins through dominant negative effect, limiting the therapeutic
533 efficacy of gene therapy[11,12,38]. In this work, we showed that sup-tRNA could
534 address these challenges by simultaneously restoring full-length p53
535 expression while converting dominant-negative truncations into functional
536 variants. Notably, the generation of enhanced suppressor p53 mutants (Figures
537 S14-S15) through specific amino acid substitution suggests a promising
538 strategy to overcome the therapeutic limit imposed by the transcriptional activity
539 of wild-type p53.
540
541 Moreover, we have developed a tailored framework for sup-tRNA in addressing
542 'undruggable' tumor suppressor mutations[4,5,10,39]. The computational pipeline,
543 which incorporates analysis of readthrough efficiency and structural
544 perturbation, could be adapted to other frequently mutated tumor suppressors
545 such as RB1, PTEN, APC and STK-11 (Figures 1F-1G and S11). Unlike
546 development of traditional small molecules targeting specific mutant proteins,
547 the sup-tRNA strategy is not restricted by protein type and mutation type, as we
548 presented that designed sup-tRNAs could overcome all three types of
549 nonsense mutations across various tumor suppressor genes.
550

551 Here we report that the super-tRNA and superb-tRNA strategy could overcome
552 nonsense mutations and restore neutral or advantageous p53 variants with
553 enhanced anti-cancer function (Figure S15). An immense collection of genomic
554 research has demonstrated that proteins can harbor rare advantageous
555 mutations. However, neutral and advantageous mutations in *TP53* have
556 received far less attention compared to extensively investigated deleterious
557 mutations, despite it reports that approximately half of all p53 variants are
558 neutral mutations[31]. This provides ample space for the application of the super-
559 tRNA and superb-tRNA strategy. As the super-tRNA therapy for *TP53* nonsense
560 mutations, we particularly recommend using $tRNA^{Gln}_{UAG}$ to suppress TAG
561 nonsense codon where the original amino acid is glutamate or tryptophan, and
562 using $tRNA^{Arg}_{UGA}$ to suppress TGA nonsense codon where the original amino
563 acid is serine or tryptophan, with the assistance of computational tools.
564 Significantly, we also remind that these strategies should be used with caution
565 for the nonsense mutations at evolutionarily conserved residues.
566
567 Recent research have demonstrated that sup-tRNA exhibited extremely low or
568 even no readthrough in normal termination codons, demonstrating the high
569 safety profile of sup-tRNA[25,26]. Consistently, our study showed that sup-
570 $tRNA^{Arg}_{UGA}$ and sup-$tRNA^{Gln}_{UAG}$ induced efficient readthrough in nonsense
571 mutations with no detectable toxicity *in vitro* and *in vivo* (Figures S19-S23).
572 However, in addition to the classical role of tRNAs as mRNA decoders, certain
573 tRNAs could respond to external perturbations and regulate gene expression[40]
574 which either promotes or suppresses tumor progression[41,42]. As engineered
575 from natural tRNAs, certain sup-tRNAs are in theory capable of driving or
576 inhibiting cancer development beyond the readthrough of nonsense
577 mutations[41,42], suggesting excluding tumor proliferation-related tRNAs in sup-
578 tRNA engineering for cancer therapy.
579
580 Overall, this study opens a new avenue for precision oncology that goes beyond

581 the oncogene-centric paradigm. By translating the concept of tumor suppressor
582 restoration into a viable therapeutic strategy, tRNA-based therapy could
583 ultimately redefine treatment strategies for the majority of human cancers
584 driven by suppressor protein inactivation.

585 **RESOURCE AVAILABILITY**

586 **Lead contact**

587 Requests for further information and resources should be directed to and will
588 be fulfilled by the lead contact, Qing Xia (xqing@hsc.pku.edu.cn).

589 **Materials availability**

590 Requests for materials will be made available by the lead contact with a
591 materials transfer agreement.

592 **Data and code availability**

593 This paper does not report original code. Any additional information required to
594 reanalyze the data reported in this paper is available from the lead contact upon
595 request.

596 **ACKNOWLEDGMENTS**

597 We are grateful to Y. Zhao and S. Shu for comments and feedbacks on this
598 article. This work was financially supported by the National Key R&D Program
599 of China, Frontier Biotechnology, (Grant No. 2023YFC3403300) and the
600 National Natural Science Foundation of China (Grant No. U23A20106).

601 **AUTHOR CONTRIBUTIONS**

602 Q.X. and B.K. conceived the idea and designed the experiments. B.K. and Z.Z.
603 performed the experiments and offered the original data. B.K., Z.D., Y.Y., and
604 Y.S. provided materials for plasmid cloning. B.K., Z.M., Y.L. and J.L. conducted
605 the animal experiments. B.K., Z.Z. and Q.X. organized the results and wrote
606 the manuscript. All authors participated in data discussion and interpretation.
607 Q.X. supervised the study.

608 **DECLARATION OF INTERESTS**

609 Q.X. and B.K. are inventors on patents regarding the suppressor tRNA for tumor
610 suppressor protein recovery. Q.X. is the founder of QiXia Decode
611 Biotechnology Co., Ltd. and holds equity in this company. The other authors
612 declare no competing interests.

613 **STAR METHODS**

614 **The tumor suppressor gene mutations**

615 The tumor suppressor gene mutation data was downloaded from the COSMIC
616 database (https://cancer.sanger.ac.uk/cosmic) and IntOGen database
617 (https://www.intogen.org/). Data of amino acid types of nonsense mutations in
618 tumor suppressor genes collected from the COSMIC database, including *TP53*
619 (COSMIC gene: COSG501), *RB1* (COSMIC gene: COSG16), *PTEN* (COSMIC
620 gene: COSG15) and *APC* (COSMIC gene: COSG257430).

621 **Plasmid construction**

622 Tumor suppressor genes (*TP53, RB1, PTEN, APC*) were constructed in the
623 pCAGGS-FLAG-GUSB-myc-T2A-GFP plasmid. pCAGGS vector has a unique
624 promoter combination of chicken β-actin promoter and CMV enhancer (CAG
625 promoter), enabling high-level expression in a wide range of cell types.
626 Subsequently, targeted mutations were achieved by introducing primers
627 containing mismatched bases during PCR to obtain plasmids with site-specific
628 nonsense mutations. The tRNAs were constructed in pcDNA3.1(+) vectors and
629 their expression was initiated by the 7SK promoter. tRNA gene sequences were
630 compiled from GtRNA database (http://gtrnadb.ucsc.edu/). PG13-luc (wt p53
631 binding sites) plasmid (Addgene ID: 16442) were purchased from Addgene. We
632 next changed the luciferase reporter to the mCherry reporter to obtain the
633 plasmid PG13-mCherry (Addgene ID: 195291). The lactic acid probe pcDNA-
634 FiLa-Cyt and pcDNA-FiLa-C-Cyt were gifts from Prof Yi Yang of East China

635 University of Science and Technology.

636 **Luciferase assay**

637 The dual luciferase reporter expresses the Firefly luciferase and Renilla
638 luciferase (as transfection control), we inserted the TAG, TAA and TGA stop
639 codons between the Firefly and Renilla reporter genes to obtain a dual-
640 fluorescent reporter system with nonsense mutations. The nonsense mutation
641 dual luciferase reporter plasmid was co-transfected with sup-tRNA plasmid into
642 HEK293T cells. The luciferase was detected using the dual luciferase reporter
643 assay kit (Promega, USA) after 48 hours of transfection.

644 **Cell culture and transfection**

645 Human HEK293T cells (ATCC CRL-11268) were cultured in DMEM medium
646 (Gibco) as suggested by the repository, supplemented with 10% fetal bovine
647 serum (FBS), 100 U/mL penicillin, 100 mg/mL streptomycin.
648 Human Calu-6 cells (ATCC HTB-56) were cultured MEM medium (Gibco) as
649 suggested by the repository, supplemented with 10% FBS, 100 U/mL penicillin,
650 and 100 mg/mL streptomycin.
651 Human Caco-2 cells (ATCC HTB-37) were cultured MEM medium (Gibco) as
652 suggested by the repository, supplemented with 20% FBS, 100 U/mL penicillin,
653 and 100 mg/mL streptomycin.
654 4T1 cells (ATCC CRL-2539) and human NCI-H460 cells (ATCC HTB-177) were
655 cultured RPMI 1640 medium (Gibco) as suggested by the repository,
656 supplemented with 10% FBS, 100 U/mL penicillin, and 100 mg/mL streptomycin.
657 Human A549 cells (ATCC CCL-185) were cultured Ham's F-12K medium (Gibco)
658 as suggested by the repository, supplemented with 10% FBS, 100 U/mL
659 penicillin, and 100 mg/mL streptomycin. The concentration of G418 Sulfate
660 used in the *in vitro* experiments was 100 ug/ml， which is supplied as a solution
661 in water was obtained from Gibco (USA).
662 All cell lines were tested to be mycoplasma-free and validated by STR profiling.

663 Plasmids were transfected using Lipo3000 and P3000 (Invitrogen). Cell
664 transfections were performed with the supplier's recommendations.

665 **Western blot analysis**

666 The equivalent of 3×10^5 cells was subjected to 10% SDS-PAGE before
667 transferring the proteins to a 0.22um PVDF membrane through eBlot® L1 Fast
668 Wet Transfer System (Genscript, USA). Membranes were incubated overnight
669 at 4 °C in the presence of a 1/200 dilution of anti-p53 antibody (DO1) (Santa
670 Cruz Biotechnology, Dallas, TX, USA; catalog number: sc-126), recognizing
671 human p53. A 1/2000 dilution of anti-P21 antibody (Proteintech, China; catalog
672 number: 10355-1-AP), a 1/100000 dilution of anti-GAPDH antibody (Proteintect,
673 China; catalog number: 1E6D9). After three washes of the membrane in TBS-
674 Tween, the membranes were exposed to a solution of horseradish peroxidase-
675 conjugated secondary antibody for detection of mouse-raised or rabbit-raised
676 antibody (Proteintect, China) at a dilution of 1/2000 (catalog number: SA00001-
677 1, SA00001-2), respectively. Antibodies were then detected with BeyoECL
678 Moon (P0018FS, Beyotime, China). Photographs were performed with 5200
679 (Tanon, Shanghai, China). The original unprocessed gel pictures are provided
680 in the source data file. Western blot results were semi-quantitatively analyzed
681 by ImageJ software. Western blot experiments were performed at least third in
682 parallel and representative results were reported. The original western blot
683 images are shown in Supplementary Figures.

684 **qRT-PCR analysis**

685 1.5×10^5 cells per well were seeded in 6-well plates in a final volume of 2 ml. On
686 the following day, cells were transfected with different plasmids of the indicated
687 drugs for 48 h. The RNA extraction was performed using the FastPure
688 Cell/Tissue Total RNA Isolation Kit V2 (Vazyme, China) according to the
689 manufacturer's recommendations. RNA was quantified using a NanoDrop
690 Spectrophotometer (Thermo Scientific, USA). cDNA was synthesized from RNA

691 using Hifair® AdvanceFast One-step RT-gDNA Digestion SuperMix for qPCR
692 (Yeasen, China). Real-time quantitative PCR was performed in the Hieff
693 UNICON® Universal Blue qPCR SYBR Green Master Mix (Yeasen, China)
694 using Roche LightCycler® 480 II (Roche, Switzerland) with the following
695 primers:
696 *GAPDH* mRNA (sense: 5′- GGAGCGAGATCCCTCCAAAAT-3′; antisense: 5′-
697 GGCTGTTGTCATACTTCTCATGG-3′).
698 *TP53* mRNA (sense: 5′- CAGCACATGACGGAGGTTGT-3′; antisense: 5′-
699 TCATCCAAATACTCCACACGC -3′).
700 *CDKN1A* mRNA (sense: 5′- TGTCCGTCAGAACCCATGC -3′; antisense: 5′-
701 AAAGTCGAAGTTCCATCGCTC -3′).
702 *BBC3* mRNA (sense: 5′- GCCAGATTTGTGAGACAAGAGG -3′; antisense: 5′-
703 CAGGCACCTAATTGGGCTC -3′).
704 *GADD45A* mRNA (sense: 5′- GAGAGCAGAAGACCGAAAGGA -3′; antisense:
705 5′- CACAACACCACGTTATCGGG -3′).
706 *BAX* mRNA (sense: 5′- CCCGAGAGGTCTTTTTCCGAG -3′; antisense: 5′-
707 CCAGCCCATGATGGTTCTGAT -3′).
708 *ZMAT3* mRNA (sense: 5′- AGAAGCCTTTTGGGCAGGAG -3′; antisense: 5′-
709 TGCTGCATAGTAATTTCGGAGTT -3′).
710 *FAS* mRNA (sense: 5′- TCTGGTTCTTACGTCTGTTGC -3′; antisense: 5′-
711 CTGTGCAGTCCCTAGCTTTCC -3′).
712 *PMAIP1* mRNA (sense: 5′- ACCAAGCCGGATTTGCGATT -3′; antisense: 5′-
713 ACTTGCACTTGTTCCTCGTGG -3′).
714 The relative expression fold was calculated by the $2^{-\Delta\Delta Ct}$ equation.

715 **PCR array**

716 Cell transfected, total RNA extracted and cDNA synthesized as described
717 above. cDNA mixed with qPCR SYBR, added into the p53 PCR Array 96- well
718 plate (WcGENE Biotech, WC-MRNA0117-H) to detect the expression of a set
719 of p53-related genes.

720 **Colony formation assay**

721 After 8 hours of transfection, we digested and resuspended the cells. We
722 planted cancer cells into the six-well plate at a density of 1000 cells/well and
723 then cultured them in a complete culture medium at 37°C for 7-10 days. After
724 being gently washed in PBS twice, the cells were fixed with 4%
725 paraformaldehyde fix solution for 30 min. Crystal Violet Staining Solution
726 (Beyotime, China; catalog number: C0121) was applied for staining the fixed
727 cells for 30 min. IncuCyte SX5 imaging system (Sartorius AG, Goettingen,
728 Germany) was used to count the number of colonies, total colonies area, and
729 individual clone area.

730 **Cell growth curve analysis**

731 Cell transfected, digested, and resuspended as described above. For the cell
732 counting, cells were inoculated into a 24-well plate with an appropriate number
733 of cells, digested at 24h, 48h, 72h, and 96h after inoculation, and then counted
734 by cell counter (Countstar BioTech, China). For the CCK-8 assays, cells were
735 seeded into a 96-well plate at 2000 cells per well. According to the protocol of
736 CCK-8 solution (Beyotime, China; catalog number: C0040), 10 μl of CCK-8
737 solution diluted in 100 μl of complete culture medium replaced the original
738 medium of each group at indicated points. After the cells were incubated in the
739 dark at 37 °C for an additional 1 h, we detected viable cells by using absorbance
740 at a 450nm wavelength through Microplate Reader AMR-100 (Allsheng, China).

741 **The landscape of gene mutation**

742 The STAR-counts data and mutation maf data of tumors were downloaded from
743 the TCGA database (https://portal.gdc.cancer.gov). The data in TPM format
744 was subsequently extracted from the STAR-counts data and normalized using
745 log2(TPM+1). The samples that had RNAseq data, maf mutation data, and
746 clinical information were then retained. The maftools package in R software was
747 utilized to download and visualize the somatic mutations of patients. Statistical

748 analysis was conducted using R software, version v4.0.3.

749 **Molecular dynamics simulation**

750 The molecular dynamics simulations of all studied protein/DNA complexes were
751 performed with the AMBER 22 molecular simulation package. The crystal
752 structure of tumor-suppressor protein p53/DNA complex (PDB code: 2AC0)
753 was used for the calculation. The starting structures of all molecular systems
754 were solvated in TIP3P water using an octahedral box, which extended 8 Å
755 away from any solute atom. To neutralize the negative charges of simulated
756 molecules, Na+ counter-ions were placed next to each negative group. MD
757 simulations were carried out by using the PMEMD module of AMBER 22. The
758 calculation began with 500 steps of steepest descent followed by 500 steps of
759 conjugate gradient minimization with a large constraint of 500 kcal mol-1 Å-2
760 on the atoms of the protein and DNA. Then 1000 steps of steepest descent
761 followed by 4000 steps of conjugate gradient minimization with no restraint on
762 the complex atoms were performed. Subsequently, after 200 ps of MD, during
763 which the temperature was slowly raised from 0 to 300 K with weak (5 kcal mol-
764 1Å-2) restraint on the protein/DNA, the final unrestrained production simulations
765 of 200.0 ns were carried out at constant pressure (1 atm) and temperature (300
766 K). In the entire simulation, SHAKE was applied to all hydrogen atoms. Periodic
767 boundary conditions with minimum image conventions were applied to calculate
768 the non-bonded interactions. A cutoff of 10 Å was used for the Lennard–Jones
769 interactions. The final respective conformations of all the protein/DNA
770 complexes used for discussion were produced from the last 50.0 ns of MD.

771 **Whole-transcriptome analysis**

772 Total RNA was extracted from tumor xenograft of different mice (three replicates
773 for each group) using TRIzol reagent. RNA libraries were constructed using the
774 VAHTS Universal V6 RNA-seq Library Prep Kit for Illumina (Vazyme, NR604-
775 02) according to the manufacturer's instructions. The concentration of the

776 extracted RNA was detected using the Nanodrop2000 (Thermo Fisher,
777 Nanodrop2000), and its integrity was tested using the Agilent 2100 (Vazyme,
778 G2939BA). The quality and quantity of the constructed libraries were assessed
779 using the BioAnalyzer 2100 system (Agilent Technologies).
780 Subsequently, the libraries were sequenced on an Illumina NovaSeq X Plus
781 platform with 150-bp paired-end reads. The sequencing data were quality-
782 controlled using the Q30 metric. After adapter trimming at the 3' end and
783 removing low-quality reads with the fastp(https://github.com/OpenGene/fastp,
784 fastp-V0.20.1), high-quality clean reads were aligned to the reference genome
785 using the HISAT2(https://daehwankimlab.github.io/hisat2/, hisat2-2.0.4).
786 Guided by the gffcompare, the ballgown software package was used to obtain
787 gene-level FPKM (Fragments Per Kilobase of transcript per Million mapped
788 reads) values as the expression profiles of mRNA. The total number of
789 expressed genes and the log2FPKM values of mRNA in different tumor
790 xenograft groups were plotted and compared. Significant differences between
791 samples were analyzed using DEseq2, and genes with a multiplicity of
792 difference FoldChange>2 times and P-value<0.01 were defined as differential
793 genes and subsequently analyzed.

794 **Preparation and characterization of LNP-tRNAs**

795 The ionizable lipid SM-102 was purchased from Guanshan Nano-Tech (China).
796 The 1,2-distearoyl-sn- glycero-3-phosphocholine (DSPC) was purchased from
797 Avanti Polar Lipids (USA); 1,2-Dimyristoyl-rac- glycero-3-methylpolyoxyethy
798 lene-2000 (DMG-PEG2000) was purchased from NOF Corporation (Japan);
799 and cholesterol (Chol) was purchased from Sigma-Aldrich (USA).
800 The molar ratio of SM102 LNPs was SM-102: DSPC: Cholesterol: DMG-
801 PEG=50:10:38.5:1.5. Nanoassemblr (Precision Nanosystems, Canada) and
802 Hamilton liquid handling system (Microlab STAR, USA) were used to prepare
803 LNPs at three volumetric portions of tRNA to 1 volumetric portion of lipid
804 solutions to obtain a lipid concentration of 2.81 mg/mL. The clean-up of the

805 crude formulations was achieved by dialysis in PBS using Slide- A-Lyzer G2
806 dialysis cassettes (Thermo Scientifc, USA).
807 Transmission Electron Microscope (TEM) image of LNPs was obtained by
808 HT7800 (HITACHI, Japan). The hydrodynamic size and zeta potential of LNPs
809 were measured by Zetasizer (Malvern, USA).

810 **Xenograft tumor model**

811 Animal experiments were proven by the Institutional Animal Care and Use
812 Committee of Peking University Health Science Center (Animal Protocol ID:
813 DLASBD0468). Female BALB/c nude mice or BALB/c mice were housed in an
814 SPF facility in a 12-h light-dark cycle and allowed free access to water and food.
815 At 7 weeks of age, BALB/c nude mice were subcutaneously inoculated with $5\times$
816 10^6 calu-6 cells or 1×10^7 caco-2 cells into the left flank, both cell lines in 50%
817 BD Matrigel™. BALB/c mice were subcutaneously inoculated with 1×10^6 4T1
818 cells into the left flank.
819 Tumor volumes and mice weight were calculated every 2 days, tumor volumes
820 using the following standard formula: volume = 0.5 × length × width^2.
821 When the tumor volume reached about 200 mm^3, treatment was initiated using
822 either LNP-tRNA (10ug tRNA/injection), LNP VECTOR, G418 (20 mg/kg/
823 injection) or D-PBS. Treatments were made by intratumor injection once every
824 4 days. When the tumor volume reaches 800mm^3, the animal is considered
825 dead and *Kapplan-Mayer* survival curves were plotted for survival analysis.
826 Maximum allowed weight loss was 10% or maximum tumor volume 1000 mm^3.
827 Mice were sacrificed after treatment. Tumors were dissected, weighed, and cut
828 in thirds: one-third was frozen in liquid nitrogen for protein analysis, one-third
829 was kept in the RNAlater (Beyotime, China; catalog number: R0118) for RT-
830 qPCR analysis and one-third was fixed in 4% paraformaldehyde (PFA) for
831 histological analysis and immunostaining.

832 **Immunofluorescence staining**

833 Collected tumors were fixed in 4% PFA at room temperature and prepared as
834 10-μm tumor sections. For p53 and CDKN1A, antigens were repaired by Tris-
835 EDTA antigen repair solution G1206 (Servicebio, Wuhan, China). For ki67,
836 PCNA and caspase-3, the antigen was repaired by Citric Acid Antigen Repair
837 Solution G1202 (Servicebio, Wuhan, China). For quenching of endogenous
838 peroxidase, the sections were incubated in 3% hydrogen peroxide solution for
839 25 min at room temperature, protected from light, and the slides were placed in
840 PBS (pH 7.4) and washed three times for 5 min each time by shaking on a
841 shaker. 3% BSA was then added to cover the tissue evenly and closed for 30
842 min at room temperature. The blocking solution was removed and sections
843 were incubated with diluted primary antibody at 4°C overnight in a wet box, 1/50
844 dilution of anti-p53 antibody (DO1) (Santa Cruz Biotechnology, Dallas, TX, USA;
845 catalog number: sc-126), recognizing human p53. 1/200 dilution of anti-P21
846 antibody (Proteintect, China; catalog number: 10355-1-AP). 1/200 dilution of
847 anti-ki67 antibody (Servicebio, China; catalog number: GB121141). 1/200
848 dilution of anti-PCNA antibody (Servicebio, China; catalog number: GB12010).
849 A 1/200 dilution of anti-cas3 antibody (Servicebio, China; catalog number:
850 GB11532). After washed in PBS on a decolorizing shaker with shaking three
851 times, 5 min each time, sections were shaken dry and the tissue was covered
852 with a drop of secondary antibody (HRP-labelled) of the corresponding species
853 to the primary antibody and incubated for 50 min at room temperature. The
854 slides were subsequently shaken dry after washing and freshly prepared DAB
855 color development solution G1212 (Servicebio, Wuhan, China) was added
856 dropwise, while the time of color development was controlled under the
857 microscope. The sections were counterstained in hematoxylin followed by
858 dehydration with graded ethanol, n-butanol, and xylene, then the sections were
859 taken out of xylene to dry and seal. The slides were photographed under
860 pathology slide scanner ws-10 (Wisleap, China). NDPView2 software

861 (Hamamatsu, Japan) was used to analyze and record these images.

862 **Histological analysis**

863 Blood samples from mice were collected from the orbital vein, and stored in the
864 tube with K2-ethylenediaminetetraacetic acid (EDTA) at 4°C. The hematological
865 parameters were analyzed using a BC-2800Vet® Auto Hematology Analyzer
866 (Shenzhen Mindray Bio-Medical Electronics Co., Ltd, Hamburg, Germany). The
867 heart, liver, spleen, lung, and kidney tissues from different groups of mice were
868 isolated and fixed in 4% PFA. They were then sequentially dehydrated in 70%,
869 95%, and 100% ethanol, followed by defatting with xylene for 2 hours before
870 being embedded in paraffin. The 10-μm-thick sections were obtained and
871 subjected to H&E staining. The slices were examined using a pathology slide
872 scanner (WS-10, Wisleap, China). Image analysis and recording were
873 performed using NDPView2 software (Hamamatsu, Japan).

874 **Statistical analysis**

875 Data were analyzed using the GraphPad Prism v5 statistical software package
876 (GraphPad Software, La Jolla, CA). Data were expressed as means ± SD or
877 SEM. The one-way analysis of variance (ANOVA) with Newman-Keuls multiple
878 comparisons test with statistical significance set at $P < 0.001$ was performed.
879 Appropriate statistical tests have been mentioned in Figure legends.

880 **REFERENCES**

881 1 Stratton, M. R., Campbell, P. J. & Futreal, P. A. (2009). The cancer genome. Nature *458*,
882 719-724, https://doi.org/10.1038/nature07943.
883 2 Martinez-Jimenez, F. et al. (2020). A compendium of mutational cancer driver genes. Nat
884 Rev Cancer *20*, 555-572, https://doi.org/10.1038/s41568-020-0290-x.
885 3 Stratton, M. R. Exploring the genomes of cancer cells: progress and promise. (2011).
886 Science *331*, 1553-1558, https://doi.org/10.1126/science.1204040 (2011).
887 4 Prasad, V. Perspective: The precision-oncology illusion.(2016). Nature *537*, S63,
888 https://doi.org/10.1038/537S63a.
889 5 Tannock, I. F. & Hickman, J. A. Limits to Personalized Cancer Medicine. (2016). N Engl J
890 Med *375*, 1289-1294, https://doi.org/10.1056/NEJMsb1607705.

6 Mendiratta, G. et al. Cancer gene mutation frequencies for the U.S. population. (2021). Nat Commun *12*, 5961, https://doi.org/10.1038/s41467-021-26213-y.

7 Mendiratta, G., Jones, M. K. & Stites, E. C. How often is each gene mutated within the cancer patient population? (2022). Mol Cell Oncol *9*, 2065176, https://doi.org/10.1080/23723556.2022.2065176.

8 Tuval, A., Strandgren, C., Heldin, A., Palomar-Siles, M. & Wiman, K. G. Pharmacological reactivation of p53 in the era of precision anticancer medicine. (2024). Nat Rev Clin Oncol *21*, 106-120, https://doi.org/10.1038/s41571-023-00842-2.

9 Brogna, S. & Wen, J. Nonsense-mediated mRNA decay (NMD) mechanisms. (2009). Nat Struct Mol Biol *16*, 107-113, https://doi.org/10.1038/nsmb.1550.

10 Dang, C. V., Reddy, E. P., Shokat, K. M. & Soucek, L. Drugging the 'undruggable' cancer targets. (2017). Nat Rev Cancer *17*, 502-508, https://doi.org/10.1038/nrc.2017.36.

11 Peuget, S., Zhou, X. & Selivanova, G. Translating p53-based therapies for cancer into the clinic. (2024). Nat Rev Cancer *24*, 192-215, https://doi.org/10.1038/s41568-023-00658-3.

12 Song, H., Xiao, S., Wu, J. & Lu, M. Drugging p53: Barriers, Criteria, and Prospects. (2024). Cancer Discov *14*, 2055-2060, https://doi.org/10.1158/2159-8290.CD-24-0837.

13 Levine, A. J. & Oren, M. The first 30 years of p53: growing ever more complex. (2009). Nat Rev Cancer *9*, 749-758, https://doi.org/10.1038/nrc2723.

14 Glimmers of Hope for Targeting p53. (2022). Cancer Discov *12*, OF5, https://doi.org/10.1158/2159-8290.CD-ND2022-0009.

15 Chen, S. et al. Arsenic Trioxide Rescues Structural p53 Mutations through a Cryptic Allosteric Site. (2021). Cancer Cell *39*, 225-239 e228, https://doi.org/10.1016/j.ccell.2020.11.013.

16 Song, H. et al. Diverse rescue potencies of p53 mutations to ATO are predetermined by intrinsic mutational properties. (2023). Sci Transl Med *15*, eabn9155, https://doi.org/10.1126/scitranslmed.abn9155.

17 Li, J. et al. Pharmacological rescue of mutant p53 triggers spontaneous tumor regression via immune responses. (2025). Cell Rep Med, *101976*, https://doi.org/10.1016/j.xcrm.2025.101976.

18 Oren, M. & Prives, C. p53: A tale of complexity and context. (2024). Cell *187*, 1569-1573, https://doi.org/10.1016/j.cell.2024.02.043.

19 Keeling, K. M. & Bedwell, D. M. Clinically relevant aminoglycosides can suppress disease-associated premature stop mutations in the IDUA and P53 cDNAs in a mammalian translation system. (2002). J Mol Med (Berl) *80*, 367-376, https://doi.org/10.1007/s00109-001-0317-z.

20 Floquet, C., Deforges, J., Rousset, J. P. & Bidou, L. Rescue of non-sense mutated p53 tumor suppressor gene by aminoglycosides. (2011). Nucleic Acids Res *39*, 3350-3362, https://doi.org/10.1093/nar/gkq1277.

21 Trzaska, C. et al. 2,6-Diaminopurine as a highly potent corrector of UGA nonsense mutations. (2020). Nat Commun *11*, 1509, https://doi.org/10.1038/s41467-020-15140-z.

22 Palomar-Siles, M. et al. Translational readthrough of nonsense mutant TP53 by mRNA incorporation of 5-Fluorouridine. (2022). Cell Death Dis *13*, 997, https://doi.org/10.1038/s41419-022-05431-2.

23 Strandgren, C. & Wiman, K. G. Therapeutic targeting of TP53 nonsense mutations in

935 cancer. (2024). Ups J Med Sci *129,* https://doi.org/10.48101/ujms.v129.10719.
936 24 Lueck, J. D. et al. Engineered transfer RNAs for suppression of premature termination
937 codons. (2019). Nat Commun *10*, 822, https://doi.org/10.1038/s41467-019-08329-4.
938 25 Wang, J. et al. AAV-delivered suppressor tRNA overcomes a nonsense mutation in mice.
939 (2022). Nature *604*, 343-348, https://doi.org/10.1038/s41586-022-04533-3.
940 26 Albers, S. et al. Engineered tRNAs suppress nonsense mutations in cells and in vivo. (2023).
941 Nature *618*, 842-848, https://doi.org/10.1038/s41586-023-06133-1.
942 27 Cheng, J. et al. Accurate proteome-wide missense variant effect prediction with
943 AlphaMissense. (2023). Science *381*, eadg7492, https://doi.org/10.1126/science.adg7492.
944 28 Bendl, J. et al. PredictSNP: robust and accurate consensus classifier for prediction of
945 disease-related mutations. (2014). PLoS Comput Biol *10*, e1003440,
946 https://doi.org/10.1371/journal.pcbi.1003440.
947 29 Kakudo, Y., Shibata, H., Otsuka, K., Kato, S. & Ishioka, C. Lack of correlation between p53-
948 dependent transcriptional activity and the ability to induce apoptosis among 179 mutant
949 p53s. (2005) Cancer Res *65*, 2108-2114, https://doi.org/10.1158/0008-5472.CAN-04-
950 2935.
951 30 Boettcher, S. et al. A dominant-negative effect drives selection of TP53 missense
952 mutations in myeloid malignancies. (2019). Science *365*, 599-604,
953 https://doi.org/10.1126/science.aax3649.
954 31 Funk, J. S. et al. Deep CRISPR mutagenesis characterizes the functional diversity of TP53
955 mutations. (2025). Nat Genet *57*, 140-153, https://doi.org/10.1038/s41588-024-02039-4.
956 32 Ventura, A. et al. Restoration of p53 function leads to tumour regression in vivo. (2007).
957 Nature *445*, 661-665, https://doi.org/10.1038/nature05541.
958 33 Xue, W. et al. Senescence and tumour clearance is triggered by p53 restoration in murine
959 liver carcinomas. (2007). Nature *445*, 656-660, https://doi.org/10.1038/nature05529.
960 34 Weinstein, I. B. & Joe, A. K. Mechanisms of disease: Oncogene addiction--a rationale for
961 molecular targeting in cancer therapy. (2006). Nat Clin Pract Oncol *3*, 448-457,
962 https://doi.org/10.1038/ncponc0558.
963 35 Weinstein, I. B. & Joe, A. Oncogene addiction. (2008). Cancer Res *68*, 3077-3080;
964 discussion 3080, https://doi.org/10.1158/0008-5472.CAN-07-3293.
965 36 Attwood, M. M., Fabbro, D., Sokolov, A. V., Knapp, S. & Schioth, H. B. Trends in kinase
966 drug discovery: targets, indications and inhibitor design. (2021). Nat Rev Drug Discov *20*,
967 839-861, https://doi.org/10.1038/s41573-021-00252-y.
968 37 Tsai, J. M., Nowak, R. P., Ebert, B. L. & Fischer, E. S. Targeted protein degradation: from
969 mechanisms to clinic. (2024). Nat Rev Mol Cell Biol *25*, 740-757,
970 https://doi.org/10.1038/s41580-024-00729-9.
971 38 Liu, Y., Su, Z., Tavana, O. & Gu, W. Understanding the complexity of p53 in a new era of
972 tumor suppression. (2024). Cancer Cell *42*, 946-967,
973 https://doi.org/10.1016/j.ccell.2024.04.009.
974 39 Sabapathy, K. & Lane, D. P. Therapeutic targeting of p53: all mutants are equal, but some
975 mutants are more equal than others. (2018). Nat Rev Clin Oncol *15*, 13-30,
976 https://doi.org/10.1038/nrclinonc.2017.151.
977 40 Torrent, M., Chalancon, G., de Groot, N. S., Wuster, A. & Madan Babu, M. Cells alter their
978 tRNA abundance to selectively regulate protein synthesis during stress conditions. (2018).

979 Sci Signal *11*, https://doi.org/10.1126/scisignal.aat6409.
980 41 Pinzaru, A. M. & Tavazoie, S. F. Transfer RNAs as dynamic and critical regulators of cancer
981 progression. (2023). Nat Rev Cancer *23*, 746-761, https://doi.org/10.1038/s41568-023-
982 00611-4.
983 42 Goodarzi, H. et al. Modulated Expression of Specific tRNAs Drives Gene Expression and
984 Cancer Progression. (2016). Cell *165*, 1416-1427,
985 https://doi.org/10.1016/j.cell.2016.05.046.
986 43 Kon, E., Ad-El, N., Hazan-Halevy, I., Stotsky-Oterin, L. & Peer, D. Targeting cancer with
987 mRNA-lipid nanoparticles: key considerations and future prospects. (2023). Nat Rev Clin
988 Oncol *20*, 739-754, https://doi.org/10.1038/s41571-023-00811-9.
989 44 Yang, M. et al. Transfer RNA-derived small RNAs in tumor microenvironment. (2023). Mol
990 Cancer *22*, 32, https://doi.org/10.1186/s12943-023-01742-w.
991